Title

Complete Electrochemical Characterization and Limiting Current of Polyacetal Electrolytes

Journal

Journal of The Electrochemical Society, 169(2)

ISSN

0013-4651

Authors

Choo, Youngwoo
Snyder, Rachel L
Shah, Neel J
et al.

Publication Date

2022-02-01

DOI

10.1149/1945-7111/ac4f22

Peer reviewed

Complete Electrochemical Characterization and Limiting Current of Polyacetal Electrolytes

Journal of The Electrochemical Society, 2022 **169** 020538
1945-7111/2022/169(2)/020538/7/$40.00

Complete Electrochemical Characterization and Limiting Current of Polyacetal Electrolytes

Youngwoo Choo,[1,2] Rachel L. Snyder,[2,3] Neel J. Shah,[1,4] Brooks A. Abel,[2,3] Geoffrey W. Coates,[2,3] and Nitash P. Balsara[1,2,4,z]

[1]*Materials Sciences Division and Joint Center for Energy Storage Research, Lawrence Berkeley National Laboratory, Berkeley, California 94720, United States of America*
[2]*Joint Center for Energy Storage Research, Argonne National Laboratory, Lemont, Illinois 60439, United States of America*
[3]*Department of Chemistry and Chemical Biology, Baker Laboratory, Cornell University, Ithaca, New York 14853, United States of America*
[4]*Department of Chemical and Biomolecular Engineering, University of California, Berkeley, California 94720, United States of America*

We investigate a polyacetal-based electrolyte, poly(1,3,6-trioxocane) (P(2EO-MO)) mixed with lithium *bis*(trifluoromethanesulfonyl)imide (LiTFSI) salt, and report full electrochemical characterization of the transport parameters and a thermodynamic property in comparison to the previously reported poly(ethylene oxide) (PEO) electrolyte data [D. Gribble et al., *J. Electrochem. Soc.*, 166, A3228 (2019)]. While the steady-state current fraction (ρ_+) of P(2EO-MO) electrolyte is greater than that of PEO electrolyte in the entire salt concentration window we explored, the rigorously defined transference number using Newman's concentrated solution theory (t_+^0) appears to be similar to that of PEO electrolyte. On the basis of full electrochemical characterization, we calculate the salt concentration profile as a function of position in the cell and predict limiting current density ($i_L L$) as a function of salt concentration. Experimental data were compared to the predicted values. The non-monotonic behaviors were observed both in prediction and experimental results with offset peak positions. We find that the limiting current density of P(2EO-MO) electrolyte is systematically lower than that of PEO electrolyte in most of the salt concentrations with the exception of $r_{av} = 0.05$. It is noteworthy that even though one measure of electrolyte efficacy ($\kappa\rho_+$) is superior in P(2EO-MO) electrolyte, the limiting current density, which is another metric of electrolyte efficacy at high currents, is not greater in P(2EO-MO).
 [DOI: 10.1149/1945-7111/ac4f22]

Manuscript submitted October 27, 2021; revised manuscript received December 14, 2021. Published February 11, 2022.

Supplementary material for this article is available online

List of Symbols

a	cross-sectional area of electrolyte (cm^2)
c	molar salt concentration (mol l^{-1})
c_{av}	average salt concentration in the cell (mol l^{-1})
D	mutual salt diffusion coefficient (cm^2 s^{-1})
$Đ$	polydispersity index
F	Faraday constant (96485 C mol^{-1})
i	current density (mA cm^{-2})
i_{ss}	steady-state current (mA)
i_Ω	initial current (mA)
$i_L L$	limiting current density (mA cm^{-1})
L	electrolyte thickness (cm)
LiTFSI	lithium *bis*(trifluoromethanesulfonyl)imide
M_n	number average molecular weight (kg mol^{-1})
$M_{2EO\text{-}MO}$	Molecular weight of the 2EO-MO repeating unit (118 g mol^{-1})
m	molality (mol kg^{-1})
PEO	poly(ethylene oxide)
P(2EO-MO)	poly(1,3,6-trioxocane)
r	molar concentration of lithium ions to ether oxygens ($r = [Li^+]/[O]$)
r_{av}	average molar concentration of lithium ions in the cell
R	gas constant (8.314 J $mol^{-1}K^{-1}$)
R_b	bulk electrolyte resistance (Ω)
$R_{b,0}$	bulk electrolyte resistance measured prior to the polarization (Ω)
$R_{i,0}$	interfacial resistance measured prior to the polarization (Ω)
$R_{i,ss}$	interfacial resistance measured during the steady-state (Ω)
T	absolute temperature (K)
$T_{d,5\%}$	decomposition temperature (K)
T_g	glass transition temperature (K)
T_m	melting temperature (K)
T_h	thermodynamic factor
t	time (min)
t_+^0	cation transference number with respect to the solvent velocity
U	open-circuit voltage (V)
ΔV	constant dc potential applied across the electrolyte (V)
x	cell coordinate defined such that $x = 0$ is at the anode and $x = L$ the cathode (cm)
z_+	number of charges per cation
Greek	
γ_{+-}	mean molar activity coefficient of the salt
Φ	cell potential (V)
Φ_{ss}	steady-state potential (V)
κ	ionic conductivity (S cm^{-1})
ν_+	number of cations in the dissociated salt
ν_-	number of anions in the dissociated salt
ρ	density (g ml^{-1})
ρ_+	steady-state current fraction

Introduction

The application of electric fields on battery electrolytes results in the emergence of salt concentration gradients. This is true for salts (or other electrolytic species such as acids and bases) dissolved in either low molar mass liquids or high molar mass polymers.[1–5] The magnitude of the concentration gradients increases with increasing current density.[3,6] The limiting current density is defined as the current density at which the concentration gradient is so large that the electrolyte concentration at the negative electrode is zero.[7] If the application powered by battery requires current density greater than the limiting current density of a particular electrolyte, then the electrolyte cannot be used for that application.

[z]E-mail: nbalsara@berkeley.edu

Ion transport in battery electrolytes is governed by three transport coefficients, ionic conductivity (κ), diffusion coefficient (D) and cation transference number with respect to the solvent velocity (t_+^0), and a thermodynamic factor, T_h.[8–15] Thus far, all four parameters have only been measured in one polymer electrolyte: poly(ethylene oxide) (PEO) mixed with lithium *bis*(trifluoromethanesulfonyl)imide (LiTFSI).[16,17] One of the goals of the present study is to present measurements of all four parameters in a mixture of a poly(ether-acetal) and LiTFSI.[18]

In the general case, where κ, D, t_+^0 and T_h are functions of salt concentration, predicting the limiting current density requires numerical integration of transport equations developed by Newman.[1] In the simple case, wherein D and t_+^0 are independent of concentration, the electrolytic solution is thermodynamically ideal, and the electrodes are planar, Newman showed that the limiting current density (i_L) is given by

$$i_L L = \frac{2c_{av}DF}{1 - t_+^0} \quad [1]$$

where F is the Faraday's constant, c_{av} is the average concentration in the cell, L is the distance between electrodes.[7] Equation 1 predicts that the limiting current density increases linearly with c_{av}. While departures from linearity may be expected because the transport parameters on the right side of Eq. 1 are often functions of concentration, one expects limiting current density to increase monotonically with increasing salt concentration. All of the experimental data in the literature is consistent with this expectation.[19–21] (We limit our attention to electrolytes well-removed from the solubility limit of the salt.)[6] In this paper, we present measurements of limiting current density in a poly(ether-acetal) electrolyte. In the system, the limiting current density is a nonmonotonic function of salt concentration. We show that this complexity arises naturally due to the concentration dependence of the relevant thermodynamic and transport parameters.

Experimental

Monomer (2EO-MO) synthesis.—A general synthetic considerations and instrumentation are provided in the Supplemental Material. 1,3,6-trioxocane (2EO-MO) was synthesized following previous reports.[18,22] In a 250 ml round-bottom flask, diethylene glycol (100 g, 0.94 mol), paraformaldehyde (37.0 g, 1.22 mol, 1.30 equiv), poly(phosphoric acid) (4.00 g, 0.03 mol, 0.03 equiv), and heptane (160 ml) were combined. A Dean–Stark adapter and condenser were fitted to the flask, and the reaction mixture was stirred at 115 °C for 12 h. After cooling the reaction mixture, residual heptane was removed via rotary evaporation. The cloudy, viscous oligomeric solution was cracked at 150 °C–180 °C under high vacuum to give a crude mixture of diethylene glycol and 1,3,6-trioxocane. Fractional distillation under high vacuum at 80 °C gave clear, colorless 1,3,6-trioxocane in 70% yield. The monomer was dried over CaH_2 for 3 days, distilled, and degassed via three freeze–pump–thaw cycles. Spectral data match previous reports.[18] ^{1}H NMR (500 MHz, $CDCl_3$): δ4.57 (s, 2H), 3.50 (s, 8H) ppm. ^{13}C NMR (125 MHz, $CDCl_3$): δ 97.91, 72.58, 70.61 ppm. HRMS (DART-MS): m/z calculated for $C_5H_{10}O_3$ $[H]^+$ 119.0703; found 119.0703.

Polymer synthesis.—Under N_2 atmosphere in a glovebox, 1,3,6-trioxocane (6.00 g, 51.0 mmol), CH_2Cl_2 (25.4 ml), and a stir bar were combined in a 100 ml round-bottom flask. After instantaneous addition of $BF_3.OEt_2$ (0.13 ml, 0.02 equiv), a rubber septum was used to seal the flask. After 30 min, the reaction gelled, stirring ceased, and the solution turned increasingly pink. The reaction was quenched after 1 h using a 1:1 mixture of acetonitrile:water (40 ml). The clear/colorless crude mixture was extracted with CH_2Cl_2 (30 ml × 3), then dried with Na_2SO_4, and filtered. The reaction mixture was concentrated by removing CH_2Cl_2 via rotary evaporation to a total volume of ~30 ml. To remove macrocyclic byproducts, the solution was precipitated into hexanes (400 ml), redissolved in 30 ml of CH_2Cl_2, and precipitated again into 400 ml of cold isopropanol. The white solid polymer was dried overnight under high vacuum and isolated in 60% yield. M_n = 55.2 kg mol^{-1}, $Đ$ = 1.97. T_g = −66 °C, T_m = 39 °C. Spectral data match previous reports.[18] ^{1}H NMR (500 MHz, $CDCl_3$): δ 4.74 (s, 2H), 3.69 (m, 8H) ppm. ^{13}C NMR (125 MHz, $CDCl_3$): δ 95.73, 70.60, 67.02 ppm.

Electrolyte preparation.—The synthesized P(2EO-MO) polymers (55 kg mol^{-1}) were dried at 90 °C for 24 h under active vacuum in the glovebox antechamber to thoroughly remove residual solvent prior to use. LiTFSI salt was purchased from Sigma Aldrich and used without further purification step. LiTFSI salt was dried at 120 °C for 72 h under active vacuum in the glovebox antechamber prior to use. Electrolytes were prepared by dissolving predetermined amounts of the polymer and the LiTFSI in anhydrous acetonitrile (Sigma Aldrich) at 60 °C until completely dissolved. Subsequently, the acetonitrile was evaporated, leaving behind a homogeneously mixed polymer/salt mixture. The electrolytes were thoroughly dried at 90 °C for 24 h under active vacuum in the glovebox antechamber to remove any residual acetonitrile before used for pouch cell assembly. To directly measure the density of a polymer electrolyte, a sample was melted at 90 °C and subsequently loaded in a heated aluminum hermetic pan (TA Instrument, 40 μl), followed by sealing with a crimper press. The mass of the sample was measured by a high precision microbalance and the measurements were triplicated to minimize error.

One measure of salt concentration is r_{av}, defined as the molar ratio of the lithium ion to the oxygen atom presents in the polymer chain, $r_{av} = [Li^+]/[O]$. The range of salt concentration window we examined were from r_{av} = 0.01 to 0.13. The electrolytes with salt concentration greater than 0.13 were non-trivial to be examined due to the drastic increase of the glass transition temperature[18,23] and thus the samples cannot be vitrified by heating at the accessible temperature. All electrolytes are amorphous at 90 °C in the salt concentration window studied.

Electrochemical measurements.—All of the cell preparation steps were conducted in a glovebox with an argon environment where the H_2O and O_2 levels kept below 2 and 5 ppm, respectively. The ionic conductivity (κ) was measured by ac impedance spectroscopy using a VMP3 potentiostat (Bio-Logic). The electrolytes were sandwiched by symmetric stainless-steel shims (MTI Corporation) separated by 508 μm thick silicone spacer with a 3.175 mm diameter hole. Aluminum tabs were attached on the stainless-steel electrodes using a Kapton tape and then the cell was vacuum sealed in Showa-Denko pouch material, leaving the tab end terminals exposed. Cells were transferred into a custom-made heating stage connected to the VMP3 potentiostat and the ionic conductivity was measured in the temperature range of 30 °C–120 °C. Electrochemical impedance spectroscopy (EIS) measurement was performed in the frequency range from 1 MHz to 100 mHz at an amplitude of 80 mV. The high-frequency minimum on the Nyquist impedance plot was determined as the bulk resistance (R_b). The thickness of the electrolyte (L) was measured by micrometer after the EIS measurement was completed. Conductivity (κ) of the electrolyte was calculated by the Eq. 2.

$$\kappa = \frac{L}{aR_b} \quad [2]$$

where a represents the electrolyte area.

The steady-state cation current ratio (ρ_+) and mutual salt diffusion coefficient (D) were measured on lithium/electrolyte/lithium symmetric cells. A detailed protocol of this experiment can be found in the literature.[24] Briefly, the electrolytes were embedded in a silicone spacer (508 μm thick, 3.175 mm diameter) and sandwiched by lithium chip electrodes. Prior to use, the lithium chips were brushed to remove any

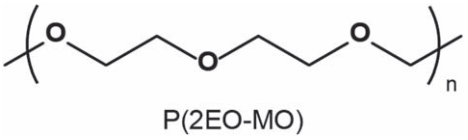

Figure 1. Chemical structure of the P(2EO-MO) used in this study.

contaminants present on the surface. Subsequently, the chips were sandwiched by a pouch material and then pressed by a pneumatic press to generate a smooth surface. Each lithium electrode was backed up by a nickel foil (~30 μm thick) and a nickel tab was attached to the nickel foil for electrical contact. The cells were vacuum sealed in the pouch material (Showa-Denko) and then transferred to a custom-built heating stage kept at 90 °C for the steady-state electrochemical measurement. Preconditioning was performed by five cycles at a low current density of 0.02 mA cm^{-2} at 90 °C to ensure the formation of uniform solid electrolyte interphase (SEI) layer. After the preconditioning, constant dc potential, ΔV, was applied until the steady-state current, i_{ss}, was reached. Bulk and interfacial resistances were measured by performing ac impedance spectroscopy before the polarization and during the steady-state. All the measurements were triplicated and the results were averaged where the error bars indicate the standard deviation.

Steady-state cation current fraction (ρ_+) was calculated by Bruce-Vincent method[25] using Eq. 3.

$$\rho_+ = \frac{i_{ss}(\Delta V - i_\Omega R_{i,0})}{i_\Omega(\Delta V - i_{ss}R_{i,ss})} \quad [3]$$

where $R_{i,0}$ and $R_{i,ss}$ are the interfacial resistances measured prior to the polarization and during the steady-state, respectively. i_Ω is defined as an initial current calculated by Ohm's law, $i_\Omega = \frac{\Delta V}{R_{i,0}+R_{b,0}}$, where $R_{b,0}$ is bulk electrolyte resistance measured prior to the polarization.

Following the polarization, the applied potential was withdrawn and cells were allowed to relax while the open-circuit voltage, U, was recorded. The time dependent voltage profile was fit to the single exponential equation depicted as

$$U(t) = k_0 + k_1 e^{-k_2 t} \quad [4]$$

where k_0 is an empirically determined offset voltage, k_1 and k_2 are the fit parameters, and t is time. The mutual salt diffusion coefficient, D, is defined as

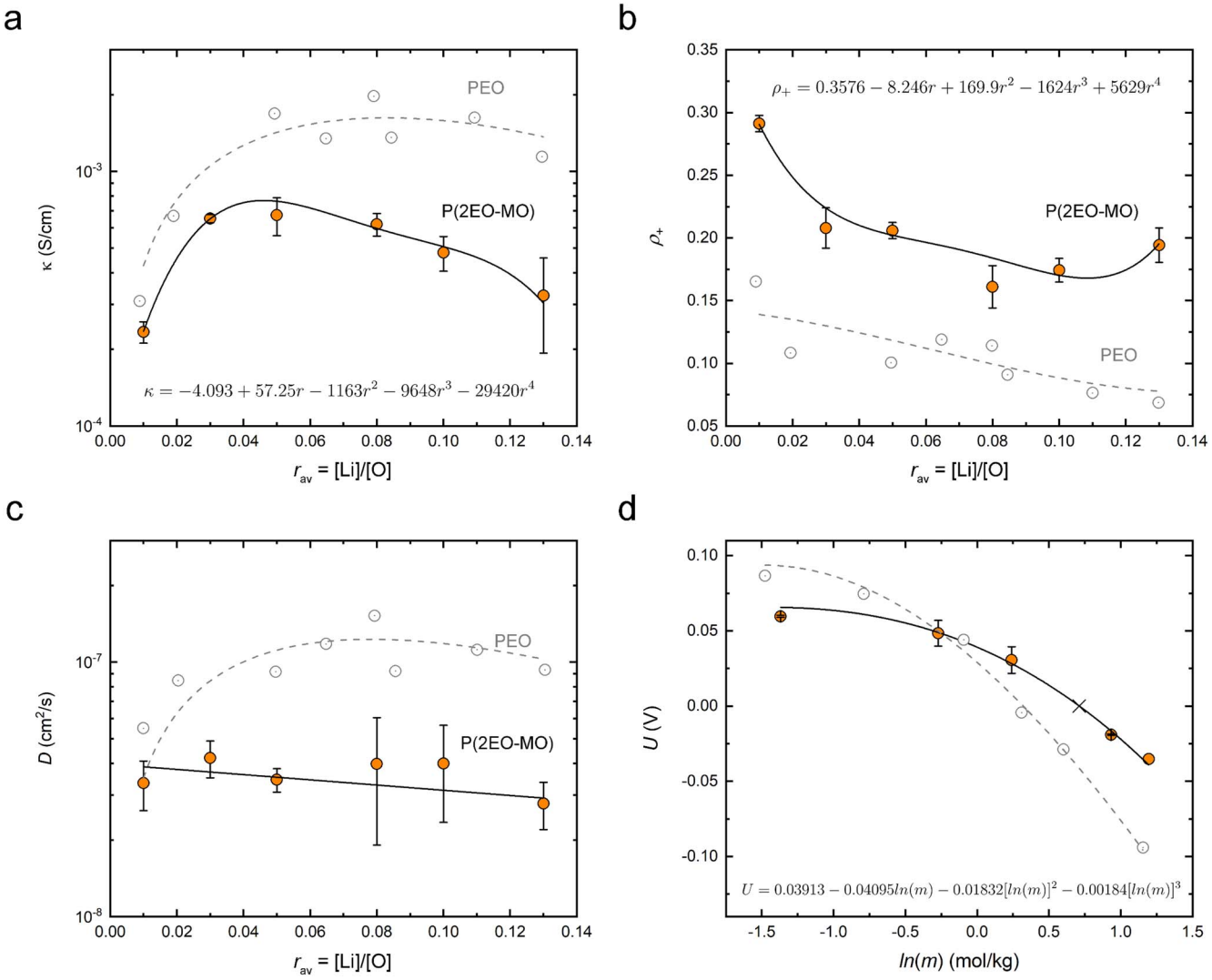

Figure 2. Ion transport properties of the P(2EO-MO) electrolytes, (a) ionic conductivity, κ, (b) cationic current fraction, ρ_+, and (c) mutual salt diffusion coefficient, D were measured at 90 °C as a function of average salt concentration r_{av}. The solid curves represent the best polynomial fits of the datasets and the fitting functions are shown. The gray data points represent the transport properties of the PEO adapted from the literature.[20] (d) The electrolyte junction potential was measured by concentration cell experiment with a reference electrolyte at $r_{av} = 0.08$ ($m = 2.034$ mol kg^{-1}).

$$D = \frac{L^2 k_2}{\pi^2} \quad [5]$$

where k_2 is the fit parameter taken from Eq. 4.

Concentration cells were prepared using the configuration similar to that described in the literature.[24] Approximately 25 mm × 4 mm channel was cut in a 508 μm thick silicone spacer and then the half of the channel was filled with reference electrolyte ($r_{ref} = 0.08$) whereas the other half was filled with electrolytes at various salt concentrations. In this way, the electrolytes with distinct salt concentrations are in contact laterally. Lithium electrodes backed with nickel foils were attached on the end of the channel and the nickel tabs were placed on the foil for electrical contact. The cells were vacuum sealed in a laminated aluminum pouch material (Showa-Denko) and then transferred into the heating stage where the cells were kept at 90 °C. The open circuit potential was measured for 120 h or until it plateaued.

Limiting current density measurement.—Lithium symmetric cells were prepared for the limiting current density measurement in a similar manner depicted above. Detailed experimental procedure is reported elsewhere.[20] After the preconditioning cycles, cells were polarized with a constant current density range from 0.05 mA cm^{-2} to 0.5 mA cm^{-2} with an increment of 0.05 mA cm^{-2} in alternating direction. Each current density was applied until the cell reaches steady-state potential, Φ_{ss}. We define the limiting current density, i_L, as the lowest current density that results the divergence of Φ_{ss}.

Results and Discussion

Poly(1,3,6-trioxocane) (P(2EO-MO)) was synthesized via cationic ring-opening polymerization of 1,3,6-trioxocane (2EO-MO) (Figure 1). $BF_3{\cdot}OEt_2$, which reacts with trace water in the reaction mixture to generate a strong acid, was used as the initiator. After purification, we obtained P(2EO-MO) with a moderate number-average molecular weight (M_n) of 55 kDa and dispersity (Đ = 1.97). The polymer shows good thermal stability by thermogravimetric analysis ($T_{d,5\%}$ = 272 °C) and demonstrates a glass transition temperature (T_g) at –66 °C and melting temperature (T_m) at 39 °C).

We measured the transport parameters of P(2EO-MO)/LiTFSI mixtures, i.e., ionic conductivity, κ, current fraction, ρ_+, and the mutual salt diffusion coefficient, D, as a function of salt concentration, r_{av}, using methods described above, and the results are shown in Figs. 2a–2c. The concentration dependencies of each transport property were fit to polynomial functions and the fit parameters are shown in insets of the Figs. 2a–2c. Also shown in these figures is the data obtained from PEO/LiTFSI mixtures taken from Ref. 20. The polynomial fits of these data are given in Ref. 20. The ionic conductivity showed nonmonotonic behavior; it increases rapidly with increasing salt concentration in the low concentration regime ($r_{av} < 0.05$) and then decreases slowly with further increase of salt concentration. Such behavior is commonly observed in both liquid and polymer electrolytes. The increase of the ionic conductivity for $r_{av} < 0.05$ is expected due to the increased concentration of the charge carriers. In the high concentration regime, i.e., $r_{av} > 0.05$, the conductivity gradually decreases which is attributed to the higher friction between polymer segments and ions. Interestingly, the peak position of the P(2EO-MO) electrolytes appears at $r_{av} \sim 0.05$ which is lower than that of the PEO electrolytes ($r_{av} \sim 0.08$).

The current fraction, ρ_+, defined by Eq. 3, as a function of salt concentration r_{av} is shown in Fig. 2b. The results indicate that ρ_+ has a nonmonotonic dependence on r_{av}, reaching a minimum of about 0.16 at $r_{av} = 0.08$. It is worth noting that ρ_+ of P(2EO-MO) is approximately two-fold higher than that of the PEO.[18]

The mutual salt diffusion coefficient, D, as a function of salt concentration r_{av} is shown in Fig. 2c. D of P(2EO-MO) is a weak function of the salt concentration. At low salt concentrations, D of P(2EO-MO) is similar to PEO. At high salt concentration, D of P(2EO-MO) is about a factor of two lower than that of PEO. We attribute this to stronger association between the ions and polymer chains in the case of P(2EO-MO). In addition, the slower segmental relaxation of P(2EO-MO), reflected by the higher glass transition temperature of P(2EO-MO), also slows down salt diffusion. Pulsed-field gradient nuclear magnetic resonance (PFG NMR) measurements of the self-diffusion coefficient of Li^+ and $TFSI^-$ ions in polyacetal electrolytes are consistent with our observation.[23]

The open-circuit potential across concentration cells, U, was measured using a reference electrolyte with salt concentration, r_{ref} = 0.08. The results are shown in Fig. 2d where U is plotted as a function of logarithm of molality, ln (m). m is calculated according to $m = \frac{3r}{M_{2EO-MO}}$, where M_{2EO-MO} is the molecular weight of the 2EO-MO repeating unit (118 g mol^{-1}). The open-circuit potential, U, decreases monotonically with increasing salt concentration, a trend that is similar to PEO. However, it is worth noting that U of P(2EO-MO) is a weaker function of salt concentration when compared to PEO.

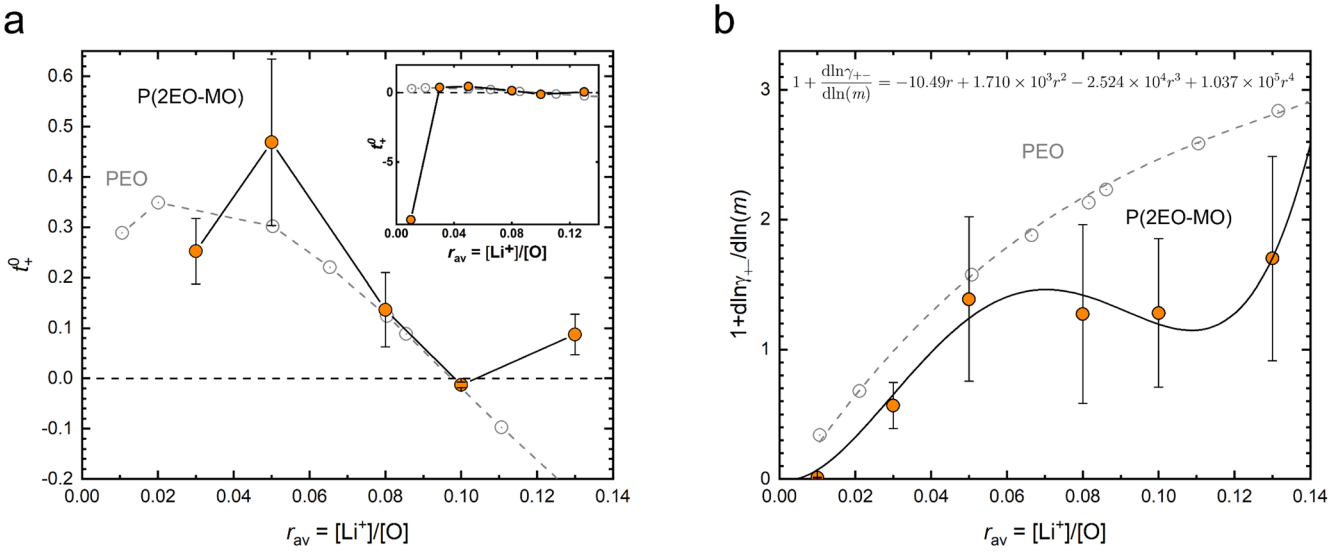

Figure 3. (a) Transference number, t_+^0, defined by concentrated solution theory as a function of salt concentration, r_{av}. The inset represents the full salt concentration range. (b) Thermodynamic factor, $1 + \frac{d\gamma_{+-}}{d\ln(m)}$, as a function of salt concentration, r_{av}. Solid lines show the best polynomial fits and the fitting functions are presented above. The gray data points represent properties of the PEO adapted from the literature.[20]

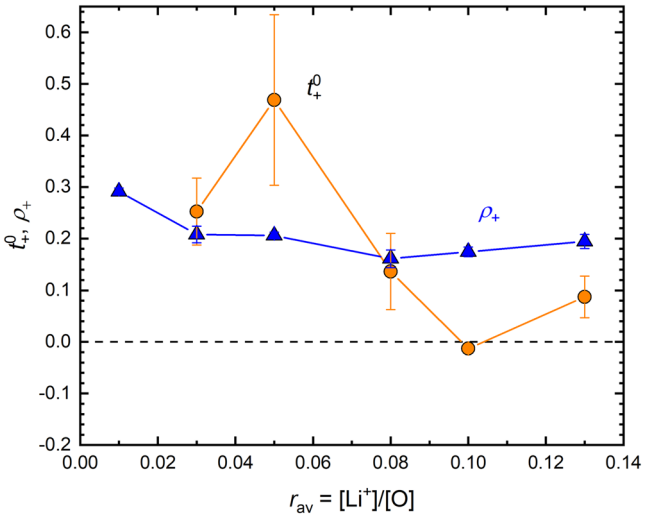

Figure 4. The concentration dependence of t_+^0 and ρ_+.

The transference number of the cation with respect to the solvent velocity defined by Newman's concentrated solution theory[7] t_+^0 is calculated by the following equation.

$$t_+^0 = 1 + \left(\frac{1}{\rho_+} - 1\right)\frac{(z_+\nu_+)2FDc}{\nu\kappa}\left(\frac{d\ \ln(m)}{dU}\right), \qquad [6]$$

where z_+ is the number of charges per cation, ν_+, ν_- are the numbers of cations and anions in the dissociated salt, respectively, $\nu = \nu_+ + \nu_-$, F is Faraday's constant, and c is the molar salt concentration. Measurements of ρ_+, κ, D and $dU/d\ln(m)$, were used to determine t_+^0 as a function of salt concentration and the results are shown in Fig. 3a. The transference number, t_+^0, is peaked at $r_{av} = 0.05$ and decreases with increasing r_{av}; t_+^0 at $r_{av} = 0.1$ is -0.01. Further increasing the salt concentration results in an increase in t_+^0; t_+^0 at $r_{av} = 0.13$ is 0.09. The dependence of t_+^0 on r_{av} of P(2EO-MO) and PEO are similar. In both cases, t_+^0 exhibits maximum followed by minimum. The minimum in PEO is -0.3 (not shown) which is significantly lower than that of P(2EO-MO). It is noteworthy that the concentration dependence of t_+^0 is very different than that of ρ_+ (Figs. 3a and 2b) indicating that the current fraction is not a good approximation of the transference number (Fig. 4).

As shown in Fig. 2d, the best polynomial fit of the open-circuit potential is given by

$$U = 0.03913 - 0.04095\ln(m) - 0.01832[\ln(m)]^2 - 0.00184[\ln(m)]^3 \qquad [7]$$

where U is expressed in V and m is expressed in moles of LiTFSI/kg of P(2EO-MO). We calculate the thermodynamic factor, $1 + \frac{d\ln(\gamma_{+-})}{d\ln(m)}$, using the relation shown in Eq. 8.

$$T_h = 1 + \frac{d\ln(\gamma_{+-})}{d\ln(m)} = -\frac{(z_+\nu_+)}{\nu}\frac{F}{RTt_-^0}\left(\frac{dU}{d\ln(m)}\right) \qquad [8]$$

where γ_{+-} is mean molar activity coefficient of the salt, R is gas constant, T is the absolute temperature, and $t_-^0 = 1 - t_+^0$. Figure 3b shows the thermodynamic factor as a function of salt concentration. For the calculation, the actual data points were used including the dilute salt concentration ($r_{av} = 0.01$). As the salt concentration increases, the thermodynamic factor peaks at $r_{av} = 0.05$ and then local minimum at $r_{av} = 0.1$ followed by increasing again at higher concentration regime.

An interesting observation is that the thermodynamic factor is lower in P(2EO-MO) over the salt concentration window that we have explored thus far. This suggests that the thermodynamic interactions between P(2EO-MO) and LiTFSI are more favorable than those between PEO and LiTFSI. It is likely that this is due to the fact that P(2EO-MO) chains have a higher density of electronegative ether oxygens. While the obvious difference between P(2EO-MO) and PEO is the density of oxygens, other factors such as polymer conformations will also play a role. Recent theoretical work based on MD simulations by Fang et al. has begun to shed light on this property. In the fullness of time, such work must be carried out to determine the underpinnings of the thermodynamic factor in P(2EO-MO).[26]

The salt concentration profile obtained at a given current density can be obtained using Eq. 9.

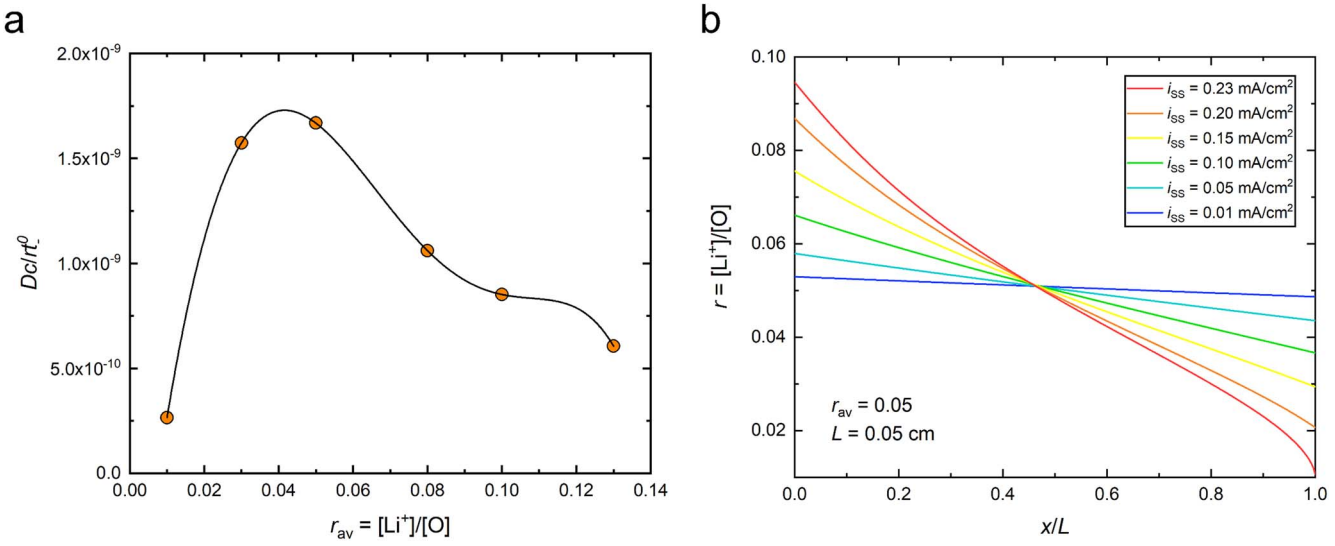

Figure 5. (a) Transport coefficient term, $(Dc)/(r_{av}t_-^0)$ is shown as a function of salt concentration (r_{av}). (b) Salt concentration profile in the P(2EO-MO) electrolyte at steady-state predicted by the model based on the concentrated solution theory. Constant dc currents were applied where the average salt concentration is $r_{av} = 0.05$.

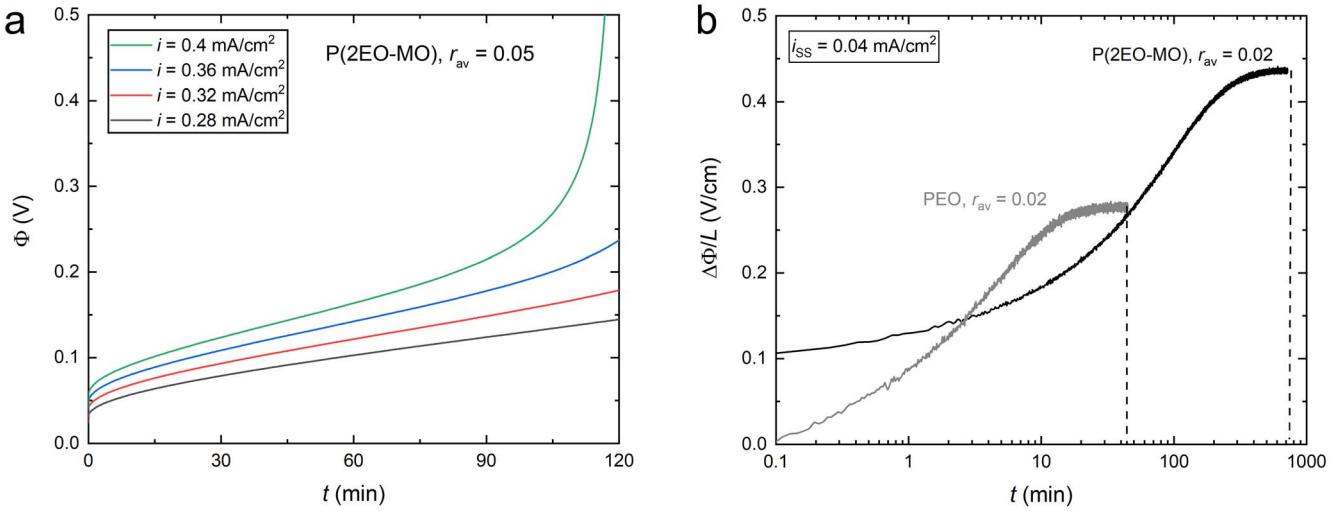

Figure 6. (a) Time dependent potential behavior of P(2EO-MO)/LiTFSI with an average salt concentration of $r_{av} = 0.05$ in response to applied current densities from $i = 0.28$ to 0.4 mA cm^{-2}. (b) Comparison of the time dependent potential behavior of PEO/LiTFSI and P(2EO-MO)/LiTFSI at low current density of $i =$ 0.04 mA cm^{-2}. The PEO data were adapted from the literature.[20]

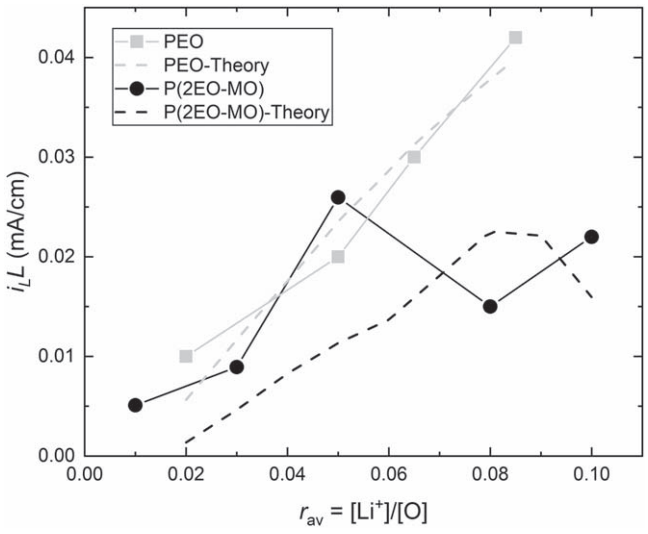

Figure 7. Limiting current density data of the PEO and P(2EO-MO) as a function of salt concentration, r_{av}. The dashed lines show the prediction based on the concentrated solution theory. PEO experimental data and predictions are based on data in Ref. 20.

$$\int_{r(x=0)}^{r(x)} \frac{D(r)c(r)}{rt_-^0(r)}dr = -\frac{iL}{F}\left(\frac{x}{L}\right) \quad [9]$$

where i is the current density in a unit of mA cm^{-2}, x is the position inside the electrolyte and L is the total thickness of the electrolyte. The detailed derivation of the Eq. 9 and related expressions can be found elsewhere.[27,28] Figure 5a shows the $(Dc)/(r_{av}t_-^0)$ of P(2EO-MO) as a function of salt concentration. Figure 5b shows the salt concentration profile calculated based on the Eq. 9 where the average salt concentration r_{av} was kept fixed at 0.05. At low current density, $i_{ss} = 0.01$ mA cm^{-2}, the salt concentration profile across the electrolyte is nearly flat. As higher current densities are applied to the cell, steeper salt concentration profiles are obtained. Eventually, at $i = 0.23$ mA cm^{-2}, the value of r at $x/L = 1$ approaches $\sim$0 indicating that the limiting current density has been reached. Repeating these calculations at different values of r_{av} enables predicting the dependence of the limiting current density on average salt concentration.

Figure 6a plots experimentally measured time-dependent cell potential, Φ, of the P(2EO-MO) electrolyte for $r_{av} = 0.05$. When the cell was polarized with $i = 0.28$ mA cm^{-2}, the cell potential gradually increases with time. In contrast, when the cell was polarized with higher current density, $i = 0.4$ mA cm^{-2}, the cell potential shoots up at $t \sim 90$ min. Following previous studies,[6] we take this to indicate that the limiting current density ($i_L L$) has been exceeded. The time chosen to for determining the limiting current density is based on practical considerations. One would like to use a time scale that is long enough to obtain a plateau in the potential vs time curves. Unfortunately, dendrite formation precludes the use of excessively long times in most electrolytes. Our use of 120 min in Fig. 6a reflects a compromise between these two factors. In Fig. 6b, we show an experiment on P(2EO-MO) with $r_{av} = 0.02$. It took about 8 h to obtain a potential vs time plateau. In contrast, a PEO electrolyte at the same concentration requires 0.5 h to reach a potential vs time plateau. It is likely that both transport and thermodynamic factors are responsible for this. The salt diffusion coefficient and the thermodynamic factor of P(2EO-MO) electrolytes are lower than those in PEO electrolytes. One thus qualitatively expect slower responses in P(2EO-MO) electrolytes. Unsteady-state models required to quantitatively predict time-dependent behavior are, however, outside the scope of this paper.

Predictions of limiting current density in P(2EO-MO) electrolytes based on the concentrated solution theory (dashed line) are compared with experimental measurements (solid discs) in Fig. 7. We plot normalized limiting current density $i_L L$ vs r_{av} in Fig. 7 to facilitate comparisons with other data that are obtained using different electrolyte thicknesses (i_L is inversely proportional to L). Interestingly, the experimentally determined limiting current density of P(2EO-MO) shows nonmonotonic behavior with a peak at $r_{av} =$ 0.05. This is qualitatively inconsistent with Eq. 1. However, the observed nonmonotonic behavior is also captured by concentrated solution theory based on independently determined transport and thermodynamic parameters. The theoretically predicted peak occurs at $r_{av} = 0.08$ which differs from the experimental value. The predicted peak value of $i_L L$, 0.25 mA cm^{-1}, is in reasonable agreement with the experimentally measured value of 0.35 mA cm^{-1}. Also shown in Fig. 7 are limiting current density predictions and measurements in PEO electrolytes. At nearly all concentrations, the PEO electrolytes exhibit higher limiting current densities.

Conclusions

We explored the electrochemical properties of a new polymer electrolyte, P(2EO-MO) with LiTFSI salt. Transport and thermodynamic parameters were determined rigorously and comparisons are made with the standard polymer electrolyte, PEO. The cation current fraction of P(2EO-MO) is higher than that of PEO, and this bodes well for performance of the electrolyte in practical devices. In spite of this, the transference numbers of the two electrolytes are similar, due to differences in the thermodynamic factor which is lower in P(2EO-MO). The conductivity and salt diffusion coefficients are lower in P(2EO-MO), and this impedes ion transport. Our main objective was to evaluate the effect of transport parameters and thermodynamic properties of P(2EO-MO) on limiting current, thereby enabling a thorough comparison with PEO electrolytes. The limiting current density is a nonmonotonic function of salt concentration, an observation is consistent with predictions based on concentrated solution theory. We find that the limiting current density of P(2EO-MO) is lower than that of PEO electrolytes at most salt concentrations; they are similar to each other at $r_{av} = 0.05$.

This study was motivated by the possibility that P(2EO-MO) may enable better performance in practical applications due to the high cation current fraction.[18,29] This detailed study shows that this is not the case. Ion transport is in fact governed by three independent transport parameters and the thermodynamic factor. It is difficult to ascertain which electrolyte may be more suited for a given application as it is unlikely that all four parameters are optimal for a given electrolyte. It is easier to ascertain the efficacy of an electrolyte is a single parameter could be used. We suggest that limiting current may be the appropriate metric for determining the optimal concentration of a given electrolyte, e.g., P(2EO-MO)/LiTFSI, and to compare the efficacy of different electrolytes.

Simple expressions for the limiting current such as Eq. 1 are often used in the literature, but they lead to the overly simplistic conclusion that the optimal electrolyte would be one with the highest concentration. The value of complete electrochemical characterization of P(2EO-MO) is the identification of the salt concentration where limiting current is maximized. This maximum is obtained both experimentally, and theoretically, based on complete characterization. Further work is needed to resolve the quantitative differences between theory and experiment.

Acknowledgments

This work was supported as part of the Joint Center for Energy Storage Research, an Energy Innovation Hub funded by the U.S. Department of Energy, Office of Science, Basic Energy Sciences.

ORCID

Youngwoo Choo https://orcid.org/0000-0003-2715-0618
Rachel L. Snyder https://orcid.org/0000-0002-0569-0704
Brooks A. Abel https://orcid.org/0000-0002-2288-1975
Geoffrey W. Coates https://orcid.org/0000-0002-3400-2552
Nitash P. Balsara https://orcid.org/0000-0002-0106-5565

References

1. Y. Ma, M. Doyle, T. F. Fuller, M. M. Doeff, L. C. De Jonghe, and J. Newman, *J. Electrochem. Soc.*, **142**, 1859 (1995).
2. J. Fawdon, J. Ihli, F. L. Mantia, and M. Pasta, *Nat. Commun.*, **12**, 4053 (2021).
3. H.-G. Steinrück et al., *Energy Environ. Sci.*, **13**, 4312 (2020).
4. K. Xu, *Chem. Rev.*, **104**, 4303 (2004).
5. J. Maier, *Electrochim. Acta*, **129**, 21 (2014).
6. D. B. Shah, H. K. Kim, H. Q. Nguyen, V. Srinivasan, and N. P. Balsara, *The Journal of Physical Chemistry C*, **123**, 23872 (2019).
7. J. Newman and N. P. Balsara, *Electrochemical Systems* (Wiley, New York, NY) (2021).
8. N. P. Balsara and J. Newman, *J. Electrochem. Soc.*, **162**, A2720 (2015).
9. L. Onsager, *Ann. N.Y. Acad. Sci.*, **46**, 241 (1945).
10. J. Landesfeind and H. A. Gasteiger, *J. Electrochem. Soc.*, **166**, A3079 (2019).
11. M. Doyle, T. F. Fuller, and J. Newman, *J. Electrochem. Soc.*, **140**, 1526 (1993).
12. M. Doyle, J. Newman, A. S. Gozdz, C. N. Schmutz, and J. M. Tarascon, *J. Electrochem. Soc.*, **143**, 1890 (1996).
13. P. Arora, M. Doyle, A. S. Gozdz, R. E. White, and J. Newman, *J. Power Sources*, **88**, 219 (2000).
14. U. S. Kim, C. B. Shin, and C.-S. Kim, *J. Power Sources*, **189**, 841 (2009).
15. V. Srinivasan and J. Newman, *J. Electrochem. Soc.*, **151**, A1517 (2004).
16. I. Villaluenga, D. M. Pesko, K. Timachova, Z. Feng, J. Newman, V. Srinivasan, and N. P. Balsara, *J. Electrochem. Soc.*, **165**, A2766 (2018).
17. K. W. Gao and N. P. Balsara, *Solid State Ionics*, **364**, 115609 (2021).
18. Q. Zheng, D. M. Pesko, B. M. Savoie, K. Timachova, A. L. Hasan, M. C. Smith, T. F. Miller, G. W. Coates, and N. P. Balsara, *Macromolecules*, **51**, 2847 (2018).
19. J. D. Bazak, J. P. Allen, S. A. Krachkovskiy, and G. R. Goward, *J. Electrochem. Soc.*, **167**, 140518 (2020).
20. D. A. Gribble, L. Frenck, D. B. Shah, J. A. Maslyn, W. S. Loo, K. I. S. Mongcopa, D. M. Pesko, and N. P. Balsara, *J. Electrochem. Soc.*, **166**, A3228 (2019).
21. S.-I. Lee, U.-H. Jung, Y.-S. Kim, M.-H. Kim, D.-J. Ahn, and H.-S. Chun, *Korean J. Chem. Eng.*, **19**, 638 (2002).
22. K. W. Gao, W. S. Loo, R. L. Snyder, B. A. Abel, Y. Choo, A. Lee, S. C. M. Teixeira, B. A. Garetz, G. W. Coates, and N. P. Balsara, *Macromolecules*, **53**, 5728 (2020).
23. D. M. Halat et al., *Chem. Mater.*, **33**, 4915 (2021).
24. D. M. Pesko, K. Timachova, R. Bhattacharya, M. C. Smith, I. Villaluenga, J. Newman, and N. P. Balsara, *J. Electrochem. Soc.*, **164**, E3569 (2017).
25. P. G. Bruce and C. A. Vincent, *J. Electroanal. Chem. Interfacial Electrochem.*, **225**, 1 (1987).
26. C. Fang, W. S. Loo, and R. Wang, *Macromolecules*, **54**, 2873 (2021).
27. D. M. Pesko, Z. Feng, S. Sawhney, J. Newman, V. Srinivasan, and N. P. Balsara, *J. Electrochem. Soc.*, **165**, A3186 (2018).
28. L. Frenck, V. D. Veeraraghavan, J. A. Maslyn, A. Müller, A. S. Ho, W. S. Loo, A. M. Minor, and N. P. Balsara, *Solid State Ionics*, **358**, 115517 (2020).
29. R. L. Snyder, Y. Choo, K. W. Gao, D. M. Halat, B. A. Abel, S. Sundararaman, D. Prendergast, J. A. Reimer, N. P. Balsara, and G. W. Coates, *ACS Energy Lett.*, **6**, 1886 (2021).